PCCP

ROYAL SOCIETY OF CHEMISTRY

PAPER

View Article Online
View Journal | View Issue

Cite this: *Phys. Chem. Chem. Phys.*, 2024, **26**, 5907

Highly efficient and fast modulation of magnetic coupling interaction in the $SrCoO_{2.5}/La_{0.7}Ca_{0.3}MnO_3$ heterostructure†

Huihui Ji,‡[abc] Siqi Wang,‡[c] Guowei Zhou,*[c] Xuanchi Zhou,[c] Jiarui Dou,[c] Penghua Kang,[c] Jingsheng Chen*[bd] and Xiaohong Xu*[c]

Received 12th November 2023,
Accepted 23rd January 2024

DOI: 10.1039/d3cp05487j

rsc.li/pccp

Effective manipulation of magnetic properties in transition-metal oxides is one of the crucial issues for the application of materials. Up to now, most investigations have focused on electrolyte-based ionic control, which is limited by the slow speed. In this work, the interfacial coupling of the $SrCoO_{2.5}$/$La_{0.7}Ca_{0.3}MnO_3$ (LCMO) bilayer is effectively modulated with fast response time. After being treated with diluted acetic acid, the bilayer changes from antiferromagnetic/ferromagnetic (AFM/FM) coupling to FM/FM coupling and the Curie temperature is also effectively increased. Meanwhile, the corresponding electric transport properties are modulated within a very short time. Combined with the structure characterization and X-ray absorption measurements, we find that the top $SrCoO_{2.5}$ layer is changed from the antiferromagnetic insulator to the ferromagnetic metal phase, which is attributed to the formation of the active oxygen species due to the reaction between the protons in the acid and the $SrCoO_{2.5}$ layer. The bottom LCMO layer remains unchanged during this process. The response time of the bilayer with the acid treatment method is more than an order of magnitude faster than other methods. It is expected that this acid treatment method may open more possibilities for manipulating the magnetic and electric properties in oxide-based devices.

Introduction

The manipulation of the magnetic properties of transition metal oxides has shown promise for improving the performance in electric devices.[1–6] A prototypical method to control the magnetic properties is to modulate the carrier concentration by an electric field. For instance, Ohno *et al.* first reported that the magnetism and the Curie temperature (T_C) in the ferromagnetic semiconductors can be modified by the electric field through changing the hole concentration.[7] Recently, electrolytic gating has been used to modify the properties of the materials because the ionic liquid can generate a considerable electric field.[6] Lu *et al.* reported the reversible three phase transformation with rich functionalities in the strontium cobaltate oxides by ionic-liquid gating (ILG),[8] which have shown great potential in neuromorphic computing.[9] Furthermore, researchers have used ILG to induce the reversible structural transformation in the $LaSrMnO_3/SrIrO_3$ heterostructure with associated electric, optical, and magnetic phase transitions, which are absent in the constituent oxides and superlattice.[10] Additionally, the low-frequency inductively coupled plasma technology was employed to induce topotactic metal–insulator transitions in the $La_{1-x}Sr_xMnO_3$ thin films.[11] The misfit strain, chemical doping, and high temperature annealing were also used to regulate the material performance.[12–16] However, there is an obvious limitation of these methods, which require long process times to achieve the desired results (*i.e.*, several minutes to hours).

Very recently, an acid solution with rich protons has been reported to trigger the rapid phase transition within seconds,[17,18] which is attributed to the migration of the active oxygen species into the materials assisted by protons. The brownmillerite $SrCoO_{2.5}$ (B-SCO) with an oxygen-vacancies channel exhibits an oxygen-dependent topotactic phase transition. This enables B-SCO to be transformed to the perovskite $SrCoO_{3-x}$ (P-SCO, $0 \leqslant x \leqslant 0.25$) accompanied by a change from antiferromagnetic insulator to ferromagnetic metal.[14,17,19,20] In this work,

[a] College of Physics, Chongqing University, Chongqing 401331, China
[b] NUS (Chongqing) Research Institute, Chongqing 401123, China
[c] School of Chemistry and Materials Science of Shanxi Normal University & Key Laboratory of Magnetic Molecules and Magnetic Information Materials of Ministry of Education, Taiyuan 03000, China. E-mail: xuxh@sxnu.edu.cn, zhougw@sxnu.edu.cn
[d] Department of Materials Science and Engineering, National University of Singapore, Singapore 117575, Singapore. E-mail: msecj@nus.edu.sg

† Electronic supplementary information (ESI) available. See DOI: https://doi.org/10.1039/d3cp05487j

‡ Huihui Ji and Siqi Wang contributed equally to this work.

the B-SCO/LCMO bilayer was fabricated on a $SrTiO_3$ substrate. The exchange bias effect is observed because of the interaction of the antiferromagnetic layer with the ferromagnetic layer. After immersing the bilayer into diluted acetic acid within 2 seconds, the bilayer changes from AFM/FM coupling (exchange bias effect) to FM/FM coupling, in which the magnetic hysteresis loop shows a two-step feature. With the assistance of protons in the acid solution, the active oxygen migrates from the surface of the B-SCO layer to the top B-SCO layer, which results in the formation of ferromagnetic P-SCO. Additionally, the bilayer was also treated with ILG as the reference experiment. Similar results were obtained but it takes a longer time. This study is expected to provide an alternative method to tune the properties of materials at a faster processing time.

Experimental section

Sample fabrication

The B-SCO (20 u.c.)/LCMO (40 u.c.) bilayer was epitaxially grown on the $SrTiO_3$ (STO) (001) substrate by a pulsed laser deposition. The deposition temperature was kept at 750 °C. The bottom LCMO and the top B-SCO layer were deposited at the oxygen pressure of 150 and 100 mTorr, respectively. Then, the deposited bilayer was *in situ* annealed for 1 h and cooled down to room temperature. Single B-SCO (40 u.c.), LCMO (40 u.c.), and P-SCO (40 u.c.) films, as well as the P-SCO (20 u.c.)/LCMO (40 u.c.) bilayer were also grown with the same deposition conditions as the references. Except for the single B-SCO film with *in situ* annealing, the other reference samples were annealed at an oxygen partial pressure of 700 torr for obtaining the perovskite structure. During the deposition, reflection high-energy electron diffraction (RHEED) was used to monitor the quality and thickness of the samples.

Structural characterization and properties measurements

The crystal structures of the samples were measured using the X-ray diffraction spectra (XRD). The superconducting quantum interference device (SQUID) was used to characterize the magnetic properties, including the magnetic hysteresis loops (M–H) and the temperature-dependent moment (M–T). The M–H measurement was conducted at 5 K with the magnetic field along the in-plane direction. Furthermore, T_C is defined as the peak of the dM/dT curve obtained from the first derivative of the M–T curve. The resistance as a function of temperature was investigated in a linear four-probe configuration through a physical properties measurement system (PPMS) within the range of 5 to 300 K. The X-ray absorption spectrum (XAS) was used to measure the Co oxidation state at beamline 08U1A of the Shanghai Synchrotron Radiation Facility at room temperature. The diluted acetic acid (0.1 mol L^{-1} acetic acid, HAc) and *N*,*N*-diethyl-*N*-(2-methoxyethyl) *N*-methylammonium bis-trifluoromethylsulfonyl-imide (DEME–TFSI) were used to induce the topotactic phase transition of the top B-SCO layer in the B-SCO/LCMO bilayer. Before the measurements, the samples were treated using deionized water and ethyl alcohol.

Results and discussion

Fig. 1(a) describes the experimental setup to trigger rapid topotactic phase transition of the top B-SCO layer in the B-SCO/LCMO bilayer. Firstly, the single B-SCO film was used to confirm the feasibility of the method. After immersing the

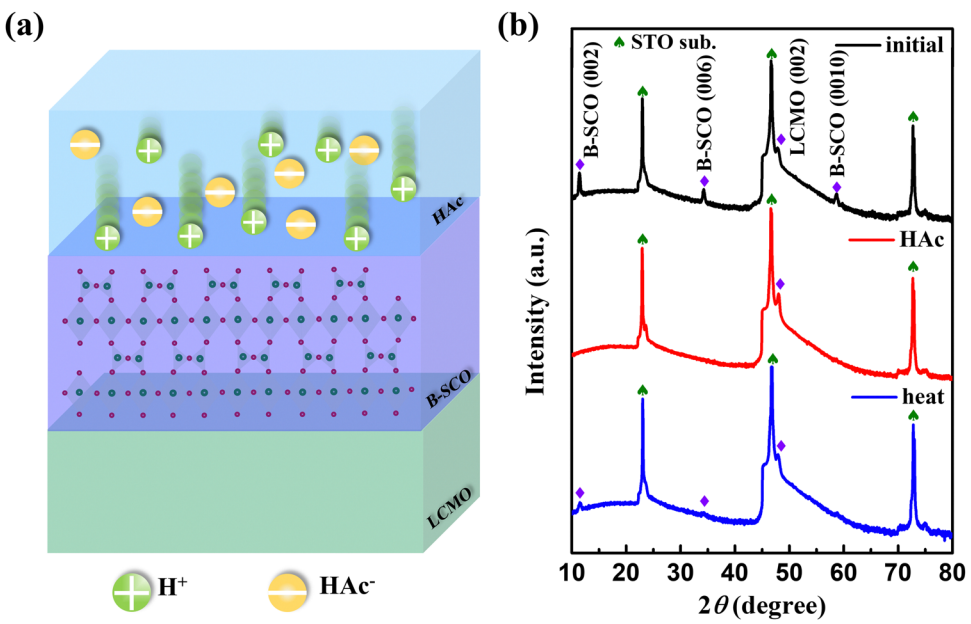

Fig. 1 (a) Schematic illustration of a rapid topotactic phase transition of the top B-SCO layer to P-SCO films of B-SCO/LCMO bilayer in a diluted HAc solution. (b) Comparison of the X-ray diffraction spectra of the B-SCO/LCMO bilayer under different states. The green spades and purple rhombuses represent the peaks of the sample and the substrate, respectively.

single B-SCO films into HAc solution for 2 seconds, the active oxygen species would be produced, which is attributed to the reaction between the proton in the acidic solutions and the surface of the B-SCO layer.[17,18] Then, the active oxygen species migrate to the inner of the B-SCO layer to fill possible oxygen vacancies, inducing the transformation to a perovskite structure. The changes in the magnetic and structural properties before and after the treatment with acid confirm the structural transition (see ESI,† Fig. S1 and S2).

Based on the above results, we develop a highly efficient pathway to tune the magnetic coupling interaction in the $SrCoO_{2.5}/LaCaMnO_3$ heterostructure. Fig. 1(b) demonstrates the XRD spectra of the B-SCO/LCMO bilayer under the different conditions. For the as-deposited bilayer (initial state, black line in Fig. 1(b)), the (002), (006) and (0010) characteristic diffraction peaks of the B-SCO layer are detected and the diffraction peak of LCMO (002) is also observed at 47.8°. After treating the bilayer in HAc at room temperature, a significant change is observed in the XRD spectra (red line in Fig. 1(b)). The diffraction peaks of the B-SCO layer disappear and only the diffraction peak of the LCMO layer still remains. Since the lattice parameters of LCMO are close to that of P-SCO film, it is expected that the diffraction peaks from LCMO and P-SCO are overlapped. We will confirm the overlap by the other characterizations. It has been reported that P-SCO is thermodynamically unstable compared to B-SCO.[14,21] Therefore, when the same sample is heated at relatively low temperature (140 °C) in an ambient atmosphere, the perovskite/perovskite structure of the bilayer would revert to the initial brownmillerite/perovskite structure. As shown in Fig. 1(b), except for the diffraction peak of LCMO, the diffraction peak of the B-SCO layer re-emerges.

Considering the correlation between the structure and the physical properties of the films,[19,22,23] we investigate the magnetic properties and the electric transport of the bilayer for the different states. In Fig. 2(a)–(c), the magnetic hysteresis loops for B-SCO/LCMO are shown for three states at 5 K and the magnetic-field cooling at ±5 T is applied along the in-plane direction from 300 to 5 K. It should be also noted that the magnetization of the bilayer consisting of antiferromagnetic B-SCO and ferromagnetic LCMO bilayer is mainly determined by the bottom LCMO layer. As shown in Fig. 2(a), the B-SCO/LCMO bilayer under the initial state exhibits a negative exchange bias effect. The *M–H* curves are shifted along the horizontal magnetic field axis and the offset direction is in the opposite direction to the cooling field. The corresponding exchange bias field (H_{EB}) is about 95 Oe. This effect is related with the pinning from the antiferromagnetic B-SCO to ferromagnetic LCMO layers. Interestingly, in the HAc-treated bilayer, the shape of the *M–H* curve is changed and shows a two-step magnetic transition (see ESI,† Fig. S3), which is due to different coercivities for the composite materials. Similar results have been observed in the other system, such as the hard $La_{0.7}Sr_{0.3}CoO_3$/soft $LaSrMnO_3$ heterostructure.[24,25] Compared with the antiferromagnetic B-SCO layer, the P-SCO layer is hard ferromagnetic with the coercivity field of 3100 Oe (see ESI,† Fig. S4(a)), while the coercivity field of the LCMO layer is about 398 Oe (see ESI,† Fig. S5(a)). Therefore, the two-step magnetic transition in the magnetic hysteresis loops is attributed

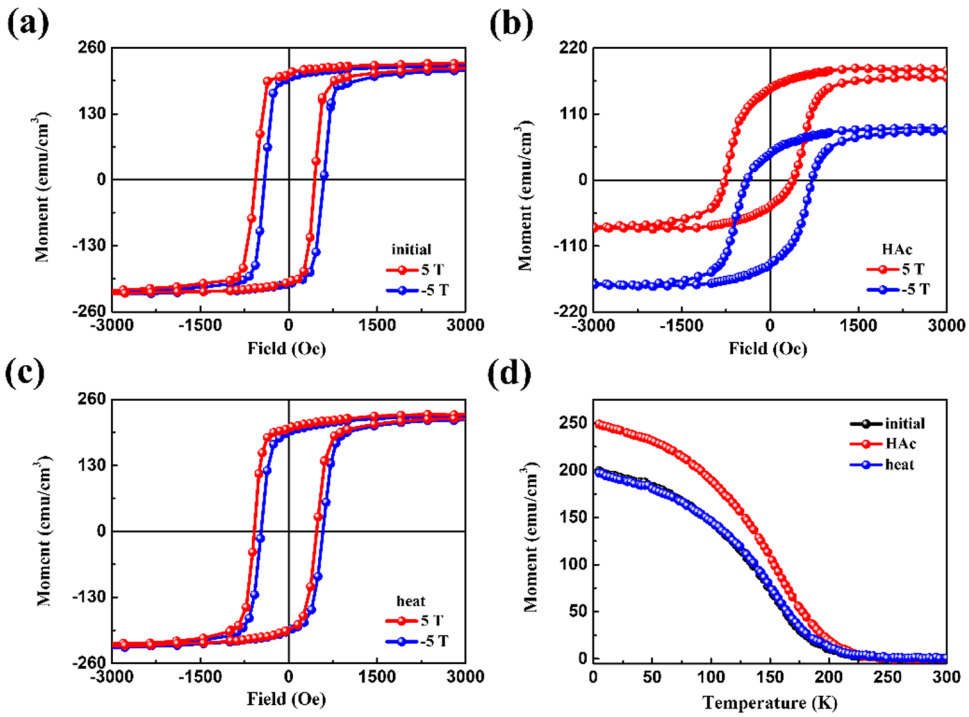

Fig. 2 Magnetic coupling variation of B-SCO/LCMO samples under different states. Magnetic hysteresis loops for B-SCO/LCMO at the initial state (a), P-SCO/LCMO with HAc treatment (b), and after heating (c). (d) Temperature dependent moment of different samples.

to a field-driven independent magnetization reversal process from LCMO and P-SCO layers. To further clarify the origin of the change, we have conducted a minor *M–H* loop of the HAc-treated bilayer as shown in Fig. 2(b), in which the sweep magnetic field is with the range of ±3000 Oe. Since the spin of the upper hard P-SCO layer remains unchanged and the magnetic moment of the soft LCMO layer reverses with the external magnetic field, the *M–H* curve shows a vertical and lateral shift. The *M–H* curve of the as-grown P-SCO/LCMO bilayer, as shown in Fig. S6 (see ESI†), further confirms the proposed magnetization reversal. Therefore, the *M–H* curves are in line with the phenomenon that the B-SCO/LCMO bilayer has been changed to a P-SCO/LCMO layer at this stage and the system shows FM/FM coupling. Furthermore, Fig. 2(c) plots the magnetic hysteresis loops of the same sample after heating. It is found that the *M–H* curves are generally restored to their initial shapes, while the exchange bias effect of the bilayer re-emerges, indicating a recovery of the top layer in the bilayer to the brownmillerite structure. In addition to this, Fig. 2(d) demonstrates the moment *versus* temperature curve of the bilayer at different states. Interestingly, the T_C of the HAc-treated bilayer is improved compared with the initial state. This may be due to the variation of the coupling interaction in the bilayer.

The electric transport properties of SCO change alongside its topotactic phase transition. Therefore, the temperature dependence of resistance amongst the three states of the bilayer was investigated, as plotted in Fig. 3(a). Remarkably, the initial B-SCO/LCMO bilayer displays the metal–insulator transition near 150 K (black line in Fig. 3(a)),[26,27] which corresponds to T_C of the single LCMO layer, as shown in Fig. S5(b) (see ESI†). This result is consistent with the magnetic measurement in which the transport behavior is mainly contributed by the LCMO layer although the top B-SCO layer shows insulating behavior. Compared with the initial/heating bilayer, the resistance of the HAc-treated sample is significantly decreased due to the top layer change to the metallic P-SCO, attributed to the injection of active oxygen species. However, the temperature of the metal–insulator transition in the bilayer moves in the high temperature direction. This behavior can also be resolved from the XAS measurement. Fig. 3(b) demonstrates the comparison of the Co valence states for all the bilayers. The peak of the Co L_3-edge of the HAc-treated sample is higher than that of the initial B-SCO/LCMO bilayer, indicating that the valence state of Co^{3+} changes to Co^{4+} through the phase transition.[28–30] This result confirms that the perovskite $SrCoO_x$ phase was formed at this stage. Remarkably, the Co valence states shift to lower energy during the HAc-treated sample returning to the initial state after heating. Overall, the B-SCO/LCMO bilayer changes to a P-SCO/LCMO bilayer after treatment by the acid. Meanwhile, the magnetic coupling interaction and the electric transport of the B-SCO/LCMO bilayer can be efficiently modulated in a fast way.

The previous studies have reported that the electric field can drive the topotactic phase transition of SCO by means of the ILG method.[6,8,19,20] After applying a negative voltage, the electric double layer is formed at the interface consisting of the ionic-liquid and surface of B-SCO films.[31–33] Thus, the negatively-charged oxygen ions can inject into the B-SCO films and fill the oxygen vacancies, inducing a transformation to the P-SCO phase. Based on this phenomenon, the ionic-liquid-gating experiment was also conducted as a reference. Fig. 4(a) shows the ILG setup for the B-SCO/LCMO bilayer. After applying −3 V on the as-deposited B-SCO/LCMO bilayer (the initial state) for 1 hour, the exchange bias effect (H_{EB} = 106 Oe, black line) disappears. Meanwhile, the shape of the *M–H* curve changes from one magnetic transition to two transitions with the different field (read line in Fig. 4(b) and Fig. S7, see ESI†). The magnetic measurement results are similar to that obtained with HAc treatment (Fig. 2(b) and Fig. S3, see ESI†). Hence, this work indirectly confirms that the B-SCO/LCMO bilayer can transform to a P-SCO/LCMO bilayer after HAc treatment, accompanied by the interaction changing from AFM/FM coupling

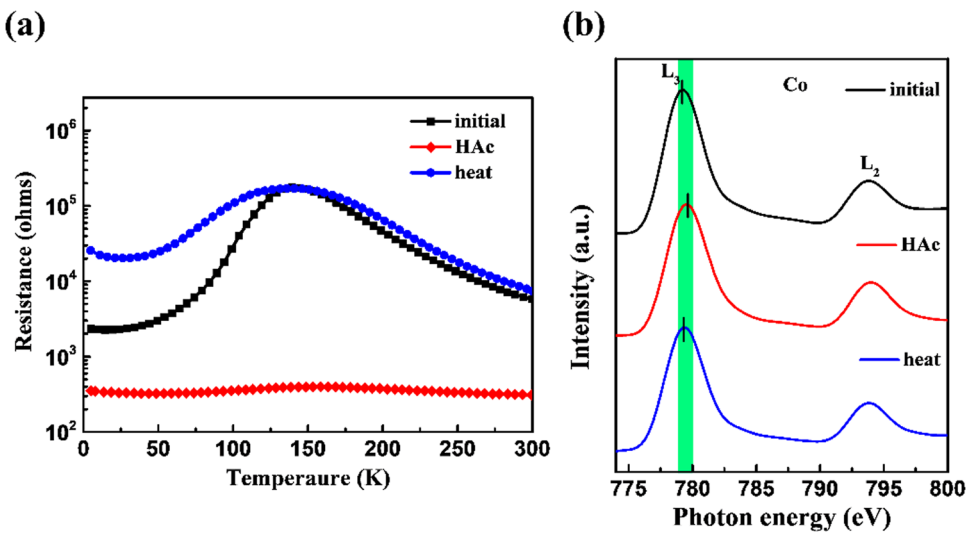

Fig. 3 (a) Resistance as a function of temperature and (b) XAS spectra of Co L-edge of the bilayer under the different states.

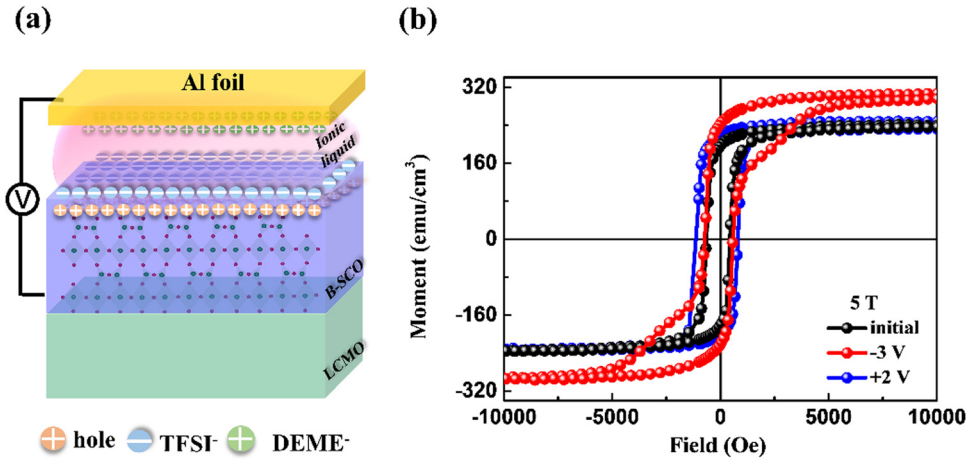

Fig. 4 (a) Schematic illustration of the device for ionic liquid gating. (b) Moment as a function of the magnetic field of the B-SCO/LCMO bilayer after being gated by different bias voltages.

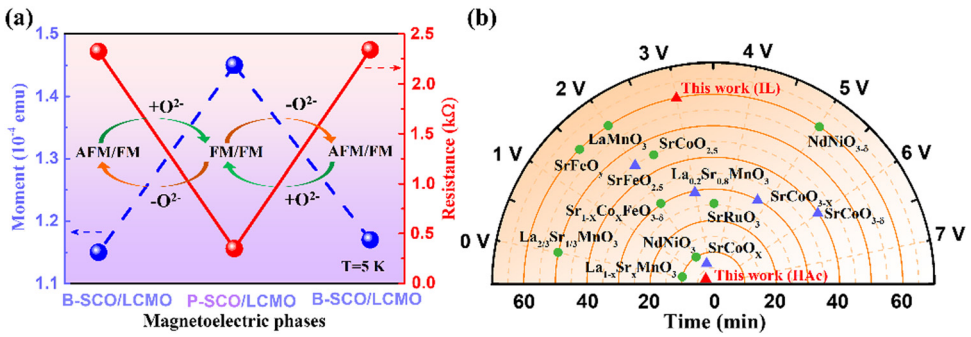

Fig. 5 (a) Evolution of the magnetic coupling and electric transport effects of the B-SCO/LCMO films under the different states at 5 K. The green and orange arrows represent the migratory direction of oxygen ions. (b) Diagram of the magnetoelectric phase transition times for different systems. The circle and triangle represent the single films and multilayer systems, respectively. For 0 V, manganite oxides were manipulated by electron-beam[16] and low-frequency coupled plasma technology.[11] In addition to this, the materials were controlled by ILG.

to FM/FM coupling. Moreover, the transition time is much faster than the ILG method.

The evolution of the magnetoelectric phase of the B-SCO/LCMO bilayer under the different states is dynamic (as shown in Fig. 5(a)). Either utilizing the ILG or HAc treatment method, the effective control of the migration direction of oxygen ions in the sample plays a vital role to induce the structural change of the B-SCO layer from the brownmillerite to the perovskite structure. Correspondingly, the magnetic and the electronic properties of the B-SCO layer are controlled simultaneously. As a result, the B-SCO/LCMO bilayer would change to a P-SCO/LCMO bilayer. And the interaction can also be facilely tuned from AFM/FM coupling to FM/FM coupling alongside the large resistance change. Additionally, utilizing the HAc-manipulated physical properties exhibits a fast response time compared with that of the other methods, as summarized in Fig. 5.

Conclusions

In summary, we have effectively manipulated the magnetic coupling interaction of the B-SCO/LCMO bilayer utilizing a fast method. The results of XRD and XAS measurement reveal that the antiferromagnetic insulating B-SCO of the top layer changes to the ferromagnetic metallic P-SCO layer after being treated by HAc. This result induces AFM/FM coupling (exchange bias effect) to FM/FM coupling, while the resistance significantly decreases. At the same time, the Curie temperature was also improved. Furthermore, the bilayer is able to transform to its initial state after the heating treatment at low temperature. The reference experiment also indirectly confirms the feasibility of this method, which takes a long time. Our result is expected to enrich the methods to manipulate physical properties and endow multifunctionalities of materials.

Author contributions

The manuscript was written through contributions of all authors. All authors have given approval to the final version of the manuscript.

Conflicts of interest

There are no conflicts to declare.

Acknowledgements

The authors would like to acknowledge the financial support by the National Natural Science Foundation of China (no. 12174237, 52171183, 51901118, and 51871137), the 1331 Engineering of Shanxi Province, the Research Project Supported by Shanxi Scholarship Council of China (2021-093), and Project funded by China Postdoctoral Science Foundation (no. 2023M730422). We also acknowledge the XAS measurements at Beamline BL08U1A in the Shanghai Synchrotron Radiation Facility (SSRF) and the XLD measurement at Beamline BL12-a in the National Synchrotron Radiation Laboratory (NSRL).

References

1 J. Hwang, Z. Feng, N. Charles, X. R. Wang, D. Lee, K. A. Stoerzinger, S. Muy, R. R. Rao, D. Lee and R. Jacobs, Tuning perovskite oxides by strain: Electronic structure, properties, and functions in (electro) catalysis and ferroelectricity, *Mater. Today*, 2019, **31**, 100–118.

2 L. Liu, Q. Qin, W. Lin, C. Li, Q. Xie, S. He, X. Shu, C. Zhou, Z. Lim and J. Yu, Current-induced magnetization switching in all-oxide heterostructures, *Nat. Nanotechnol.*, 2019, **14**, 939–944.

3 A. G. Ricciardulli, S. Yang, J. H. Smet and M. Saliba, Emerging perovskite monolayers, *Nat. Mater.*, 2021, **20**, 1325–1336.

4 L. Liu, G. Zhou, X. Shu, C. Li, W. Lin, L. Ren, C. Zhou, T. Zhao, R. Guo and Q. Xie, Room-temperature spin-orbit torque switching in a manganite-based heterostructure, *Phys. Rev. B*, 2022, **105**, 144419.

5 G. Zhou, H. Ji, Z. Yan, M. Cai, P. Kang, J. Zhang, J. Lu, J. Zhang, J. Chen and X. Xu, Interfacial engineering manipulation of magnetic anisotropy evolution *via* orbital reconstruction in low-dimensional manganite superlattices, *Sci. China Mater.*, 2022, **65**, 1902–1911.

6 Y. Guan, H. Han, F. Li, G. Li and S. S. P. Parkin, Ionic Gating for Tuning Electronic and Magnetic Properties, *Annu. Rev. Mater. Res.*, 2023, **53**, 25–51.

7 H. Ohno, D. Chiba, F. Matsukura, T. Omiya, E. Abe, T. Dietl, Y. Ohno and K. Ohtani, Electric-field control of ferromagnetism, *Nature*, 2000, **408**, 944–946.

8 N. Lu, P. Zhang, Q. Zhang, R. Qiao, Q. He, H.-B. Li, Y. Wang, J. Guo, D. Zhang, Z. Duan, Z. Li, M. Wang, S. Yang, M. Yan, E. Arenholz, S. Zhou, W. Yang, L. Gu, C.-W. Nan, J. Wu, Y. Tokura and P. Yu, Electric-field control of tri-state phase transformation with a selective dual-ion switch, *Nature*, 2017, **546**, 124–128.

9 X. Mou, J. Tang, Y. Lyu, Q. Zhang, S. Yang, F. Xu, W. Liu, M. Xu, Y. Zhou and W. Sun, Analog memristive synapse based on topotactic phase transition for high-performance neuromorphic computing and neural network pruning, *Sci. Adv.*, 2021, **7**, eabh0648.

10 D. Yi, Y. Wang, O. M. J. van't Erve, L. Xu, H. Yuan, M. J. Veit, P. P. Balakrishnan, Y. Choi, A. T. N'Diaye, P. Shafer, E. Arenholz, A. Grutter, H. Xu, P. Yu, B. T. Jonker and Y. Suzuki, Emergent electric field control of phase transformation in oxide superlattices, *Nat. Commun.*, 2020, **11**, 902.

11 S. Chen, H. Zhou, X. Ye, Z. Chen, J. Zhao, S. Das, C. Klewe, L. Zhang, E. Lupi and P. Shafer, Versatile and highly efficient controls of reversible topotactic metal–insulator transitions through proton intercalation, *Adv. Funct. Mater.*, 2019, **29**, 1907072.

12 L. Cao, O. Petracic, P. Zakalek, A. Weber, U. Rücker, J. Schubert, A. Koutsioubas, S. Mattauch and T. Brückel, Reversible Control of Physical Properties *via* an Oxygen-Vacancy-Driven Topotactic Transition in Epitaxial $La_{0.7}Sr_{0.3}MnO_{3-\delta}$ Thin Films, *Adv. Mater.*, 2019, **31**, 1806183.

13 S. Hu and J. Seidel, Oxygen content modulation by nanoscale chemical and electrical patterning in epitaxial $SrCoO_{3-\delta}$ ($0 < \delta \leq 0.5$) thin films, *Nanotechnology*, 2016, **27**, 325301.

14 H. Jeen, W. S. Choi, J. W. Freeland, H. Ohta, C. U. Jung and H. N. Lee, Topotactic Phase Transformation of the Brownmillerite $SrCoO_{2.5}$ to the Perovskite $SrCoO_{3-\delta}$, *Adv. Mater.*, 2013, **25**, 3651–3656.

15 J. Li, M.-X. Guan, P.-F. Nan, J. Wang, B.-H. Ge, K.-M. Qiao, H.-R. Zhang, W.-H. Liang, J.-Z. Hao and H.-B. Zhou, Topotactic phase transformations by concerted dual-ion migration of B-site cation and oxygen in multivalent cobaltite La–Sr–Co–O_x films, *Nano Energy*, 2020, **78**, 105215.

16 L. Yao, S. Majumdar, L. Äkäslompolo, S. Inkinen, Q. H. Qin and S. van Dijken, Electron-Beam-Induced Perovskite–Brownmillerite–Perovskite Structural Phase Transitions in Epitaxial $La_{2/3}Sr_{1/3}MnO_3$ Films, *Adv. Mater.*, 2014, **26**, 2789–2793.

17 S. Lu, F. Yin, Y. Wang, N. Lu, L. Gao, H. Peng, Y. Lyu, Y. Long, J. Li and P. Yu, Facile Pathways to Synthesize Perovskite Strontium Cobalt Oxides, *Adv. Funct. Mater.*, 2023, **33**, 2210377.

18 Q. Wang, Y. Gu, C. Chen, L. Qiao, F. Pan and C. Song, Realizing Metastable Cobaltite Perovskite *via* Proton-Induced Filling of Oxygen Vacancy Channels, *ACS Appl. Mater. Interfaces*, 2022, **15**, 1574–1582.

19 H. Ji, Z. Yan, G. Zhou, P. Kang, Z. Li and X. Xu, Electric field-controlled reversible high-temperature perpendicular magnetic anisotropy in cobaltate–manganite heterostructures, *J. Mater. Chem. C*, 2022, **10**, 12844–12852.

20 H. Ji, G. Zhou, X. Wang, J. Zhang, P. Kang and X. Xu, Electric-Field Reversible Switching of the Exchange Spring and Exchange Bias Effect in $SrCoO_{3-x}/La_{0.7}Sr_{0.3}MnO_3$ Heterostructures, *ACS Appl. Mater. Interfaces*, 2021, **13**, 15774–15782.

21 Q. Zhang, G. Hu, V. Starchenko, G. Wan, E. M. Dufresne, Y. Dong, H. Liu, H. Zhou, H. Jeen and K. Saritas, Phase transition dynamics in a complex oxide heterostructure, *Phys. Rev. Lett.*, 2022, **129**, 235701.

22 G. Zhou, H. Ji, Z. Yan, P. Kang, Z. Li and X. Xu, Dimensionality control of magnetic coupling at interfaces of cuprate–manganite superlattices, *Mater. Horiz.*, 2021, **8**, 2485–2493.

23 W. Liu, L. Liu, B. Cheng, H. Qin, G. Zhou, B. Cui and J. Hu, Electrical Control of Magnetism through Proton Migration in Fe_3O_4/Graphene Heterostructure, *Nano Lett.*, 2022, **22**, 4392–4399.

24 A. M. Kane, I. T. Chiu, N. J. Ahlm, R. V. Chopdekar, A. T. N'Diaye, E. Arenholz, A. Mehta, V. Lauter and Y. Takamura,

Controlling Magnetization Vector Depth Profiles of $La_{0.7}Sr_{0.3}CoO_3/La_{0.7}Sr_{0.3}MnO_3$ Exchange Spring Bilayers *via* Interface Reconstruction, *ACS Appl. Mater. Interfaces*, 2020, **12**, 45437–45443.

25 B. Li, R. Chopdekar, E. Arenholz, A. Mehta and Y. Takamura, Unconventional switching behavior in $La_{0.7}Sr_{0.3}MnO_3/La_{0.7}Sr_{0.3}CoO_3$ exchange-spring bilayers, *Appl. Phys. Lett.*, 2014, **105**, 202401.

26 Z. Zhang, J. Shao, F. Jin, K. Dai, J. Li, D. Lan, E. Hua, Y. Han, L. Wei, F. Cheng, B. Ge, L. Wang, Y. Zhao and W. Wu, Uniaxial Strain and Hydrostatic Pressure Engineering of the Hidden Magnetism in $La_{1-x}Ca_xMnO_3$ ($0 \leq x \leq 1/2$) Thin Films, *Nano Lett.*, 2022, **22**, 7328–7335.

27 C. J. Lu, Z. L. Wang, C. Kwon and Q. X. Jia, Microstructure of epitaxial $La_{0.7}Ca_{0.3}MnO_3$ thin films grown on $LaAlO_3$ and $SrTiO_3$, *J. Appl. Phys.*, 2000, **88**, 4032–4043.

28 H. Jeen, W. S. Choi, M. D. Biegalski, C. M. Folkman, I. C. Tung, D. D. Fong, J. W. Freeland, D. Shin, H. Ohta, M. F. Chisholm and H. N. Lee, Reversible redox reactions in an epitaxially stabilized $SrCoO_x$ oxygen sponge, *Nat. Mater.*, 2013, **12**, 1057–1063.

29 J. Zhao, Y. Luo, J.-O. Wang, H. Qian, C. Liu, X. He, Q. Zhang, H. Huang, B. Zhang, S. Li, E. Guo, C. Ge, T. Yang, X. Li, M. He, L. Gu, K.-J. Jin, K. Ibrahim and H. Guo, Electronic structure evolutions driven by oxygen vacancy in $SrCoO_{3-x}$ films, *Sci. China Mater.*, 2019, **62**, 1162–1168.

30 S. Ning, Q. Zhang, C. Occhialini, R. Comin, X. Zhong and C. A. Ross, Voltage Control of Magnetism above Room Temperature in Epitaxial $SrCo_{1-x}Fe_xO_{3-\delta}$, *ACS Nano*, 2020, **14**, 8949–8957.

31 B. Cui, C. Song, G. A. Gehring, F. Li, G. Wang, C. Chen, J. Peng, H. Mao, F. Zeng and F. Pan, Electrical Manipulation of Orbital Occupancy and Magnetic Anisotropy in Manganites, *Adv. Funct. Mater.*, 2014, **25**, 864–870.

32 R. Scherwitzl, P. Zubko, I. G. Lezama, S. Ono, A. F. Morpurgo, G. Catalan and J. M. Triscone, Electric-Field Control of the Metal–Insulator Transition in Ultrathin $NdNiO_3$ Films, *Adv. Mater.*, 2010, **22**, 5517–5520.

33 H.-T. Zhang, Z. Zhang, H. Zhou, H. Tanaka, D. D. Fong and S. Ramanathan, Beyond electrostatic modification: design and discovery of functional oxide phases *via* ionic-electronic doping, *Adv. Phys.: X*, 2019, **4**, 1523686.